

# First-Principles study of vibrational and non-collinear magnetic properties of the perovskite to postperovskite pressure transition of NaMnF<sub>3</sub>

A. C. Garcia-Castro<sup>1,2</sup>, A. H. Romero<sup>3,2</sup> and E. Bousquet<sup>1</sup>

<sup>1</sup>*Physique Théorique des Matériaux, Université de Liège, B-4000 Sart-Tilman, Belgium*

<sup>2</sup>*Centro de Investigación y Estudios Avanzados del IPN, MX-76230, Querétaro, México. and*

<sup>3</sup>*Physics Department, West Virginia University, WV-26506-6315, Morgantown, USA.*

We performed a first-principles study of the structural, vibrational, electronic and magnetic properties of NaMnF<sub>3</sub> under applied isotropic pressure. We found that NaMnF<sub>3</sub> undergoes a reconstructive phase transition at 8 GPa from the *Pnma* distorted perovskite structure toward the *Cmcm* post-perovskite structure. This is confirmed by a sudden change of the Mn–F–Mn bondings where the crystal goes from corner shared octahedra in the *Pnma* phase to edge shared octahedra in the *Cmcm* phase. The magnetic ordering also changes from a *G*-type antiferromagnetic ordering in the *Pnma* phase to a *C*-type antiferromagnetic ordering in the *Cmcm* phase. Interestingly, we found that the high-spin *d*-orbital filling is kept at the phase transition which has never been observed in the known magnetic post-perovskite structures. We also found a highly non-collinear magnetic ordering in the *Cmcm* post-perovskite phase that drives a large ferromagnetic canting of the spins. We discuss the validity of these results with respect to the *U* and *J* parameter of the GGA+*U* exchange correlation functional used in our study and conclude that large spin canting is a promising property of the post-perovskite fluoride compounds.

PACS numbers: 31.15.A-, 71.15.Mb, 75.50.-y, 81.40.Vw

## A. Introduction

Perovskite materials with stoichiometry ABX<sub>3</sub> are well known in material sciences due to their numerous properties of high interest for technological applications. These properties are very diverse such as ferroelectricity,<sup>1</sup> ferromagnetism<sup>2</sup>, piezoelectricity<sup>3</sup>, pyroelectricity<sup>4</sup> or superconductivity.<sup>5</sup> Going further, recent researches focused on the achievement of multifunctionalities in a single material that would open the door to new types of applications such as computer memories or spintronic.<sup>6,7</sup> One of the main features of these compounds is that their properties can be conveniently tuned by external control parameters such as electric and magnetic fields, temperature, strain or pressure.<sup>8,9</sup> Hydrostatic pressure appeared to be an interesting external parameter for the understanding of the perovskite physics since they exhibit profuse structural, electronic and magnetic phase transitions.<sup>10</sup> A particularly appealing pressure phase transition is the perovskite to post-perovskite (*pPv*) phase transition that has been observed in MgSiO<sub>3</sub> crystal in 2004.<sup>11,12</sup> The discovery of this *pPv* phase transition had important consequences in the physics of the earth mantle where MgSiO<sub>3</sub> is abundant and is under very high pressure conditions.<sup>11,12</sup> The *pPv* transition has then attracted great interests and has been observed in other oxide and fluoride perovskites such as MgGeO<sub>3</sub><sup>13</sup>, CaSnO<sub>3</sub><sup>14</sup>, NaMgF<sub>3</sub><sup>15</sup> or NaCoF<sub>3</sub><sup>16,17</sup> (see Table I). Interestingly, the fluoroperovskite crystals have a lower pressure and temperature *pPv* phase transition than the oxides and thus making them attractive for the study of the *pPv* phase. Furthermore, it has been reported the possibility to keep the *pPv* phase at atmospheric pressure when releasing the pressure in fluoroperovskites<sup>18</sup> while all the oxides return to their

*Pnma* distorted perovskite ground state.<sup>16</sup> Besides the interest for the *pPv* transition in earth mantle studies, it has been recently highlighted the existence of a ferroelectric instability in the cubic phase of ABF<sub>3</sub> perovskites that originates from a geometric effect rather than a dynamical charge transfer as it the case in oxides.<sup>19</sup> It has also been shown the possibility to induce a ferroelectric polarization in NaMnF<sub>3</sub> when applying an epitaxial constraint which leads to new possibilities to make multiferroic materials within the family of fluoroperovskites. The study of the fluoroperovskites under pressure is then of high interest to scrutinize the reasons and origins of their unique properties and their potential multiferroic character.

In this paper, we propose to study from first-principles calculations the structural, electronic and magnetic properties of NaMnF<sub>3</sub> as function of applied hydrostatic pressure. The results are presented as follows. We first determine the structural ground state structures over a wide range of pressure conditions and we predict a transition from the *Pnma* ground state to a *pPv* phase that has not been explored experimentally. We analyse the *pPv* phase transition through a vibrational characterization (phonons) and a structural study. We then focus on the analysis of the magnetic behaviour with a special interest in the non-collinear magnetic ground states allowed in the *pPv*. We found a high-spin ground state associated with a large ferromagnetic canting that has not been reported in any of the previous *pPv* transition observed in other compounds. The validity of the results are discussed with respect to the values of the DFT+*U* *U* and *J* parameters.

TABLE I. Lattice parameters ( $\text{\AA}$ ) of the  $pPv$  phase and related temperature (T, in Kelvin) and pressure (P, in GPa) transitions from the  $Pnma$  phase to the  $pPv$  phase of fluoride and oxide perovskites. In the  $pPv$  phase, the  $A$  and  $B$  cations occupy the  $4a$  and  $4c$  Wyckoff positions and the O/F anions occupy the  $4c$  and  $8d$  positions. Most of the oxides have higher pressure and temperature transitions than the fluorides. \*\*This work.

Crystal	$a/b/c$	P	T	Ref
Oxides $ABO_3$				
MgSiO <sub>3</sub>	2.456/8.042/6.093	121	300	11
MgGeO <sub>3</sub>	2.613/8.473/6.443	78	300	13
MnGeO <sub>3</sub>	2.703/8.921/6.668	57 - 65	1200 - 2400	14
CaSnO <sub>3</sub>	2.854/9.343/7.090	56	300	14
CaIrO <sub>3</sub>	3.145/9.862/7.298	1 - 3	1648 - 1798	20,21
CaRuO <sub>3</sub>	3.115/9.827/7.296	21 - 25	1173 - 1373	22-24
CaPtO <sub>3</sub>	3.126/9.920/7.351	4	1073	25,26
CaRhO <sub>3</sub>	3.101/9.856/7.264	12 - 27	1273 - 1673	27,28
NaIrO <sub>3</sub>	3.040/10.358/7.177	4 - 5	1073	29
Fluorides $ABF_3$				
NaMgF <sub>3</sub>	2.716/8.381/6.849	18 - 30	300 -	15
NaZnF <sub>3</sub>	3.034/10.032/7.450	13 - 18	300 -	30
NaCoF <sub>3</sub>	3.064/10.123/7.468	11 - 14	300 -	16,17
NaNiF <sub>3</sub>	3.026/10.058/7.401	16 - 18	1273 - 1473	17,18
NaMnF <sub>3</sub>	3.042/9.839/7.416	8	0	**

## B. Computational details

Total energy calculations were performed with the Vienna Ab-initio Simulation Package (VASP)<sup>31,32</sup> and within the projected augmented wave (PAW) method to describe the valence and core electrons.<sup>33</sup> The electronic configurations taken into account in the PAW pseudopotentials are as follows: seven valence electrons for Na ( $2p^63s^1$ ), thirteen for Mn ( $3p^64s^23d^5$ ) and seven for F ( $2s^22p^5$ ). We used the Generalized Gradient Approximation (GGA) exchange correlation functional within its PBEsol variant<sup>34</sup> and we corrected it to increase the  $d$ -electron localization by means of the DFT+ $U$  approximation, with  $U = 4.0$  eV and  $J = 0$  of the Liechtenstein formalism<sup>35</sup>. Due to the magnetic character of NaMnF<sub>3</sub>, the spin degree of freedom have been included in the calculations. Non-collinear magnetism calculations have been carried out by including the spin-orbit coupling as implemented in VASP by Hobbs *et. al.*<sup>36</sup>. Different values of the  $U$  and  $J$  parameters were systematically varied to study the influence of these parameters on the results. The reciprocal space has been discretized by a Monkhorst-Pack  $k$ -point mesh of  $(6 \times 4 \times 6)$  and the plane wave expansion has been limited by an energy cut-off of 800 eV. These convergence parameters were necessary in order to have a resolution on the force of less than  $1 \times 10^{-4}$  eV/ $\text{\AA}$  and a resolution on the energy of

0.01 meV. Analysis of the optimal structure as a function of pressure was carried out according to the third-order Birch-Murnaghan equation of state (BM-EOS)<sup>37</sup> by fitting the total energy dependence of the primitive cell volume per molecule. Vibrational properties were computed through the formalism of density functional perturbation theory (DFPT)<sup>38,39</sup> as implemented in VASP and post-processed with the Phonopy code<sup>40</sup>.

## C. Structural and vibrational properties of the $Pnma$ phase of NaMnF<sub>3</sub>

At room temperature and atmospheric pressure, the sodium manganese fluoride compound NaMnF<sub>3</sub> crystallizes in the  $Pnma$  structure (space group number 62) which is composed by tilted Mn-F<sub>6</sub> octahedra along the three cubic directions and antipolar motions of the Na cations<sup>41</sup>. This is the result of the condensation of zone-boundary antiferrodistortive (AFD) unstable modes observed in the cubic reference structure phonon-dispersion curves<sup>19</sup>. By performing the structural relaxation of the atomic positions and of the cell parameters of NaMnF<sub>3</sub> in the  $Pnma$  phase, we obtain the lattice parameters  $a = 5.750$   $\text{\AA}$ ,  $b = 8.007$   $\text{\AA}$  and  $c = 5.547$   $\text{\AA}$ . This corresponds to a difference of 0.2% with respect to the experimental measurements reported by Daniel *et. al.*<sup>41</sup>.

In Tables II and III we report the calculated silent, Raman and infra-red (IR) phonon modes as well as the mode Grüneisen parameters ( $\gamma_i$ ) of the relaxed  $Pnma$  ground state. The irreducible representation of the  $Pnma$  perovskite phase is  $\Gamma = 8A_u \oplus 10B_{1u} \oplus 8B_{2u} \oplus 10B_{3u} \oplus 7A_g \oplus 5B_{1g} \oplus 7B_{2g} \oplus 5B_{3g}$ . Both the Raman ( $A_g$ ,  $B_{1g}$ ,  $B_{2g}$  and  $B_{3g}$  labels) and IR modes ( $B_{1u}$ ,  $B_{2u}$  and  $B_{3u}$  labels) are in good agreement with the available experimental reports<sup>41,42</sup>. We note that a very soft polar  $B_{2u}$  mode is present with a frequency of 18  $\text{cm}^{-1}$ . This indicates that the  $Pnma$  phase is close to a ferroelectric phase transition and this mode is responsible for the epitaxial strain induced ferroelectricity of NaMnF<sub>3</sub> reported by A. C. Garcia-Castro *et al.*<sup>19</sup> From the Grüneisen parameters reported in Table III, we observe that two phonon modes are particularly sensitive to a change in volume: the soft  $B_{2u}$  mode at 18  $\text{cm}^{-1}$  with  $\gamma = 7.957$  and the  $A_g$  mode at 79  $\text{cm}^{-1}$  with  $\gamma = 4.844$  such as they can be easily detected from Raman experiments. Two phonon modes have negative  $\gamma$  and correspond to the modes that become soft as the volume decreases, which indicates that probably these two phonon modes are close to a nearest neighbour force instability.

Regarding the magnetic ordering, the total energy differences between the ferromagnetic (FM),  $C$ - and  $A$ -type antiferromagnetic (AFM) with respect to  $G$ -type AFM ordering in the  $Pnma$  structure are respectively 79.03, 54.08 and 24.18 meV. The lowest energy is thus given by the  $G$ -type AFM ordering, in agreement with the experimental measurements that establish a  $G$ -type AFM ordering for the  $Pnma$  phase of NaMnF<sub>3</sub>.<sup>43</sup> All of that

confirms that our choice of parameters for the DFT calculations (GGA PBEsol and  $U = 4.0$  eV) of  $\text{NaMnF}_3$  gives good results when comparing to the experimental measurements.

TABLE II. Calculated Raman, Infra-red (IR) and silent modes frequencies ( $\text{cm}^{-1}$ ) of the  $Pnma$  phase of  $\text{NaMnF}_3$  (at zero pressure). In brackets are presented the experimental values of the Raman<sup>41</sup> and the IR<sup>42</sup> modes.

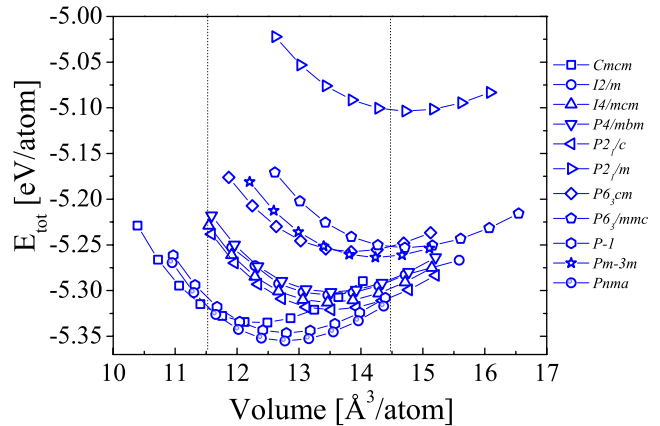
Raman modes			
$A_g$	$B_{1g}$	$B_{2g}$	$B_{3g}$
79 (88)	86 (—)	132 (140)	87 (96)
135 (143)	154 (160)	145 (155)	191 (—)
175 (183)	220 (182)	191 (201)	252 (—)
202 (212)	303 (312)	216 (226)	294 (302)
242 (250)	414 (346)	260 (—)	462 (—)
259 (270)	—	281 (293)	—
309 (319)	—	449 (—)	—
Silent		IR modes	
$A_u$	$B_{1u}$	$B_{2u}$	$B_{3u}$
59 (—)	114 (103)	18 (—)	91 (103)
114 (—)	125 (132)	118(120)	148 (132)
124 (—)	180 (161)	180 (181)	152 (161)
133 (—)	196 (194)	205 (—)	183 (208)
198 (—)	223 (228)	280 (—)	222 (220)
278 (—)	255 (256)	367 (—)	237 (256)
363 (—)	272 (289)	387 (—)	307 (289)
396 (—)	312 (—)	—	347 (—)
—	402 (—)	—	389 (—)

TABLE III. Calculated mode Grüneisen parameters ( $\gamma_i$ ) for the  $\text{NaMnF}_3$   $Pnma$  phase at  $\Gamma$  and around atmospheric pressure.

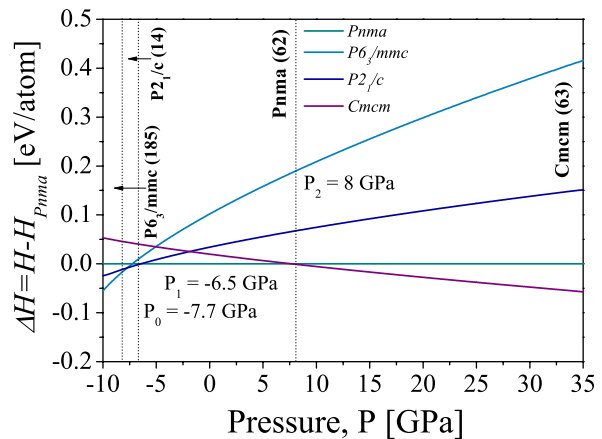
$A_g$	$B_{1g}$	$B_{2g}$	$B_{3g}$	$A_u$	$B_{1u}$	$B_{2u}$	$B_{3u}$
4.844	1.425	1.226	3.017	-1.018	1.674	7.957	1.752
0.857	1.168	2.710	1.110	-0.668	1.323	0.559	1.546
2.196	2.416	2.872	1.351	0.172	0.574	-0.139	0.486
2.273	1.714	1.401	1.833	1.692	0.707	1.663	1.717
3.063	1.023	1.855	0.897	0.990	2.983	1.274	2.252
1.706	—	1.627	—	1.512	1.980	1.632	2.632
1.417	—	0.919	—	1.713	1.884	1.507	0.906
—	—	—	—	1.452	0.992	—	1.026
—	—	—	—	—	1.421	—	1.471

#### D. Study of $\text{NaMnF}_3$ under hydrostatic pressure

In this section we study the pressure phase transitions of  $\text{NaMnF}_3$ . In order to identify the enthalpy



(a)



(b)

FIG. 1. (Color online) (a) Total energy of  $\text{NaMnF}_3$  as a function of the volume per atom for all different crystal structures.  $Cmc1$  and  $Pnma$  structures show the lowest energy values for lower volumes. (b)  $\Delta H/\text{atom}$  as a function of external pressure in  $\text{NaMnF}_3$  structures.  $Pnma$  to  $Cmc1$  structural transition can be seen at the critical pressure of 8 GPa.

ground state under hydrostatic pressure, we fitted the total energy versus the volume through the Birch-Murnaghan equation of state (BM-EOS)<sup>37</sup> for the following common structures found in perovskites:  $Cmc1$  ( $pPv$  phase),  $I2/m$ ,  $I4/mcm$ ,  $P4/mbm$ ,  $P2_1/c$ ,  $P2_1/m$ ,  $P6_3cm$ ,  $P6_3/mmc$ ,  $P1$ ,  $Pm\bar{3}m$ , and  $Pnma$ . For all of them, the  $G$ -type AFM magnetic ordering was considered in our calculations. In Fig.1a we report the total energy values per atom as a function of the volume change with respect to the equilibrium volume. As we would expect, the  $Pnma$  and  $Cmc1$ - $pPv$  structures exhibit the lowest energy values at low volumes. In order to identify the lowest energy phase, we report the enthalpy ( $H$ ), as obtained from the equation of state, versus the pressure in Fig.1b. Going from the lowest to the highest pressure, we found the following low enthalpy phases. Between -10 GPa and -8.9 GPa the hexagonal  $P6_3/mmc$  phase is

the most stable structure. Between -8.9 GPa and -6.5 GPa we found the  $P2_1/c$  structure to be the most stable. Then between -6.5 GPa and 8.0 GPa the orthorhombic  $Pnma$  structure is the ground state and thus passing through the atmospheric pressure as expected from the experimental results. At higher pressures (above 8 GPa, up to 35 GPa) the orthorhombic  $Cmcm$   $pPv$  structure is the lowest energy phase. Then, we found that  $\text{NaMnF}_3$  presents a phase transition at relatively low pressure (8 GPa) from the  $Pnma$  perovskite phase to the  $Cmcm$   $pPv$  phase.

In Fig.2a we represent a schematic view of the  $Pnma$  and the  $pPv$  phases. It is clear that the structural transition between the  $Pnma$  and the  $pPv$  phase is reconstructive since a breaking of Mn–F–Mn bonds is needed to connect the two structures. This corresponds to a transition between corner-shared octahedra in the  $Pnma$  phase to edge-shared octahedra in the  $pPv$  phase. The  $pPv$  phase can be viewed as layers of edge-shared octahedra separated by layers of Na cations along the  $y$ -direction. In Fig.2b we report the calculated X-ray diffraction patterns (XRD) for the  $Pnma$  and the post-perovskite  $Cmcm$  phases with a  $\text{Cu-K}\alpha = 1.5418 \text{ \AA}$  X-ray wavelength. The XRD pattern of the room temperature  $Pnma$  is in good agreement with the experimental reports shown as a triangles in the Fig.2b.<sup>41,42,44</sup> No experimental data exists for the  $pPv$  phase of  $\text{NaMnF}_3$  but the calculated XRD pattern fit the  $pPv$  symmetry found in other compounds such as  $\text{MgGeO}_3$ .<sup>13</sup>

An interesting parameter to be analysed in the  $Pnma$  to  $pPv$  phase transition is the dependence of the octahedral tilting angle of the  $Pnma$  structure as a function of pressure. O’Keeffe *et. al.* reported that the transition from the  $Pnma$  to the  $pPv$  structure takes place when the octahedra tilting angles reach  $25^\circ$ .<sup>45</sup> This condition is reached when the atmospheric pressure tilting angle of the  $Pnma$  phase is above  $15^\circ$ .<sup>12,45,46</sup> For this purpose, we computed the pressure dependence of the octahedra tilting angle  $\phi$  of the  $Pnma$  structure following to the relationship deduced by O’Keeffe *et. al.*<sup>45</sup> such as  $\phi = \cos^{-1}(\sqrt{2}c^2/ab)$  with  $a$ ,  $b$  and  $c$  are the cell parameters. We report our results as a function of pressure for  $\text{NaMnF}_3$  and the experimental data for  $\text{NaMF}_3$  compounds with  $M = \text{Zn, Ni, Co, Mg, and Mn}$  in Fig.2c. The experimental results for  $M = \text{Zn, Ni, Co}$  and  $\text{Mg}$  are taken from Yusa *et. al.*<sup>16</sup> Experimental data for lattice parameters used in the calculation of  $\phi$  were extracted from the report of Katrusiak *et. al.*<sup>47</sup> As it can be appreciated, all the experimental measurements follow the tilting criterion proposed by O’Keeffe, *i.e.* a  $pPv$  phase transition at  $\phi = 25^\circ$ . The experimental results for  $\text{NaMnF}_3$  (filled squares) are in good agreement with our calculations (open squares) up to 5.6 GPa (maximum pressure explored experimentally). Our calculations predict that the tilt angle reaches  $25^\circ$  at 8 GPa, where the transition should occur according to the O’Keeffe rule which is indeed in agreement with our BM-EOS prediction of 8 GPa as critical pressure.

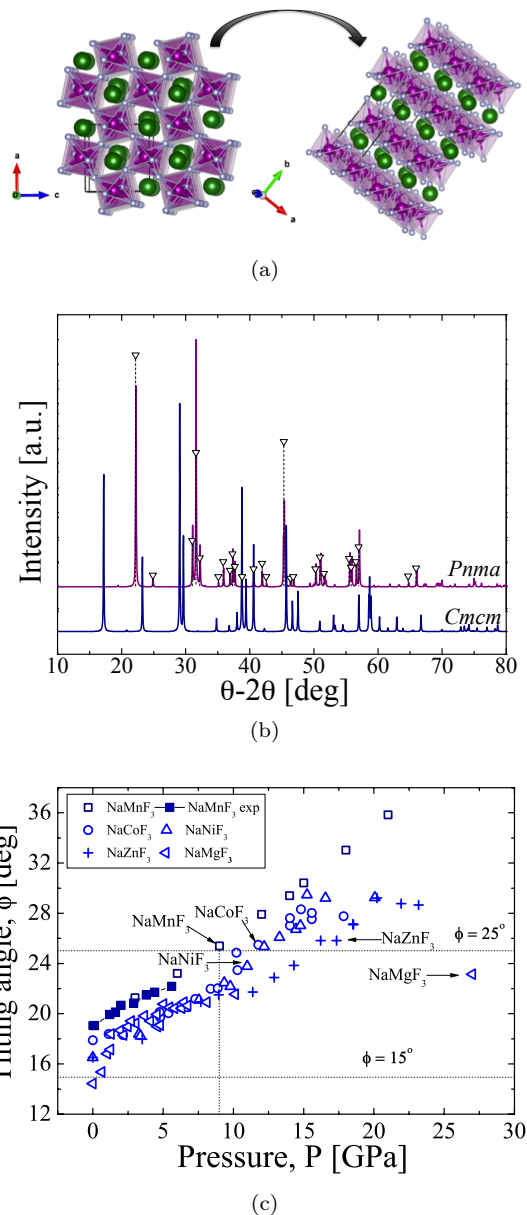


FIG. 2. (Color online) (a) Schematic view of the phase transition from  $Pnma$  to  $Cmcm$ . Na, Mn and F atoms are represented in green, violet and grey colors respectively. The breaking of bondings for the transition from corner-shared to edge-shared octahedra can be appreciated. (b) Simulated XRD patterns for  $Pnma$  and  $Cmcm$  structures. The room temperature  $Pnma$  phase is in good agreement with the experimental reports (open triangles).<sup>41,42,44</sup> (c) Octahedra tilt angle as a function of pressure in  $\text{NaMF}_3$ . For  $M = \text{Zn, Ni, Co}$  and  $\text{Mg}$  experimental results are taken from Yusa *et. al.*<sup>16</sup> All of these compounds present the transition from the  $Pnma$  to the  $Cmcm$  structures at a tilting angle close to  $25^\circ$ . Experimental results for  $\text{NaMnF}_3$  at low pressure were taken from Katrusiak *et. al.*<sup>47</sup> Full agreement between experimental (filled squares) and our theoretical calculations (empty squares) can be appreciated.

Our theoretical findings for the transition between the  $Pnma$  and the  $Cmcm$   $pPv$  phase do not follow the recent experimental report of Akaogi *et. al.*<sup>44</sup>. In their pressure measurements at high temperature ( $T = 1273$  K), Akaogi *et. al.* do not observe a transition from the  $Pnma$  to the  $pPv$  structure up to 24 GPa but found, instead, a  $MnF_2 + Na_3Mn_2F_7$  phase decomposition around 8 GPa. We note that Katrusiak *et al.* also report a transition from the  $Pnma$  to the cubic phase  $Pm\bar{3}m$  at  $T_c = 970$  K and ambient pressure<sup>47</sup> for this compound which is not observed by Akaogi *et. al.* at very high temperature (higher than  $T_c = 970$ K). We suggest that at the very high temperature where Akaogi *et. al.* performed their measurements, it is indeed possible that a phase decomposition appears such as they do not observe the  $pPv$  transition. We also remark that at such high temperature, the O’Keeffe rule is not fulfilled since the crystal is cubic or with titling angle smaller than the required critical value of  $15^\circ$  to observe the  $Pnma$  to  $pPv$  phase transition under pressure such as our calculation are still valid at low temperature. Following the experimental results and in order to understand the decomposition phases, we performed calculations for  $Na_3Mn_2F_7$  and  $MnF_2$  compounds. The first stoichiometry is the one of the Ruddlesen-Popper (RP) phases<sup>48</sup> with  $A_{n-1}A'{}_2B_nX_{3n+1}$  formula, which in our particular case corresponds to  $n = 2$  and  $A' = A = Na$ ,  $B = Mn$  and  $X = F$ . To our knowledge, there is no previous report of the sodium-manganese based compound in the RP phase. Therefore, all reported phases for similar compounds (oxides<sup>48</sup> and fluorides<sup>49</sup>) were tested and the energy minimum per structure was analysed. Nevertheless, none of our simulated XRD patterns of the considered RP phases match the one reported by Akaogi *et. al.*<sup>44</sup>, while for the  $MnF_2$  compound, we obtain a good agreement with the experiments.<sup>44</sup> We are thus confident about our predicted phase transition from the perovskite toward the  $pPv$  phase of  $NaMnF_3$  at relatively low pressure (8 GPa) and more experimental measurements would be required in order to clarify the pressure phase transition that takes place in  $NaMnF_3$  at lower (room) temperature.

We now focus on the vibrational characterization of the  $pPv$  phase at 8 GPa. In Table IV we report the computed phonon mode frequencies and the mode Grüneisen parameter ( $\gamma_i$ ) in the  $Cmcm$   $pPv$  structure with the lattice parameters relaxed at 8 GPa (also reported in Table I). The irreducible representation at the  $\Gamma$  zone center point is:  $2A_u \oplus 6B_{1u} \oplus 6B_{2u} \oplus 4B_{3u} \oplus 4A_g \oplus 3B_{1g} \oplus B_{2g} \oplus 4B_{3g}$ . Two silent modes ( $A_u$  label), sixteen IR active modes ( $B_{1u}$ ,  $B_{2u}$  and  $B_{3u}$ ) and twelve Raman active modes ( $B_{1g}$ ,  $B_{2g}$  and  $B_{3g}$ ) are thus expected. As we can see in Table IV, all the calculated modes at the  $\Gamma$  point of the BZ are positive, indicating a vibrational local stability of the  $pPv$  phase at 8GPa. The lowest frequency mode is a silent mode  $A_u$  at  $62\text{ cm}^{-1}$  and the lowest polar mode is a  $B_{1u}$  mode with a frequency of  $90\text{ cm}^{-1}$ . The obtained Grüneisen parameters are smaller than the one obtained in the  $Pnma$  ground state structure, which can

TABLE IV. Computed Raman, Infra-red and silent modes of  $NaMnF_3$  in post-perovskite  $Cmcm$  phase as well as the mode Grüneisen parameters ( $\gamma_i$ ) at  $\Gamma$  around 12 GPa.

Raman, IR and silent modes [ $\text{cm}^{-1}$ ]							
$A_g$	$B_{1g}$	$B_{2g}$	$B_{3g}$	$A_u$	$B_{1u}$	$B_{2u}$	$B_{3u}$
194	118	284	138	62	90	196	125
239	240	—	228	335	168	223	248
310	298	—	358	—	192	294	343
402	—	—	512	—	356	374	—
—	—	—	—	—	509	416	—
Mode Grüneisen parameters ( $\gamma_i$ )							
1.619	0.702	1.891	1.674	1.699	-0.137	-0.204	0.074
0.757	1.623	—	1.975	1.293	-0.204	0.449	2.011
1.265	2.107	—	1.301	—	2.558	1.427	1.384
1.050	—	—	1.171	—	1.265	0.972	—
—	—	—	—	—	1.543	1.156	—

be explained from an interatomic force stiffness larger in the  $pPv$  phase than in the  $Pnma$  phase. Even though there are some phonon modes with negative parameter, they are not large enough to have an effect on the thermal expansion. We also report in Fig.3 the evolution of the Raman and IR modes as a function of pressure from 0 GPa to 15 GPa. After the transition, the system goes to a reduced crystallographic unit cell such as the number of modes is two times smaller in the  $Cmcm$   $pPv$  phase than it is in the  $Pnma$  phase. We note that whatever the  $Pnma$  or the  $pPv$  structure, all the phonon mode frequencies harden when increasing the pressure. This is also valid for the soft  $B_{2u}$  polar mode of the  $Pnma$  structure that hardens as the pressure increases and thus in agreement with the usual behaviour of perovskites in the presence of the AFD distortions, which are inimical to the ferroelectric distortions and are enhanced with pressure.

### E. Magnetic properties of the $pPv$ phase

Before performing the non-collinear magnetic calculations, it is useful to make a preliminary symmetry analysis in order to determine the magnetic orderings that are allowed in the  $pPv$  structure. The  $Cmcm$  space group belongs to the  $D_{2h}$  point group<sup>50,51</sup> and the Mn atoms are placed at the  $4c$  Wyckoff position with coordinates  $(0,0,0)$  for  $Mn_1$ ,  $(0,0,\frac{1}{2})$  for  $Mn_2$ ,  $(\frac{1}{2},\frac{1}{2},0)$  for  $Mn_3$  and  $(\frac{1}{2},\frac{1}{2},\frac{1}{2})$  for  $Mn_4$ . From these 4 magnetic cations, we can define 4 collinear magnetic orderings depending on the sign of the magnetic moments of  $(Mn_1, Mn_2, Mn_3, Mn_4)$ :  $F$  (+, +, +, +) for the FM ordering,  $A$  (+, +, -, -) for the  $A$ -type AFM ordering,  $C$  (+, -, +, -) for the  $C$ -type AFM ordering and  $G$  (+, -, -, +) for the  $G$ -type AFM ordering, where + and - correspond to spin up and down respectively. Of course, the ferrimagnetic or-

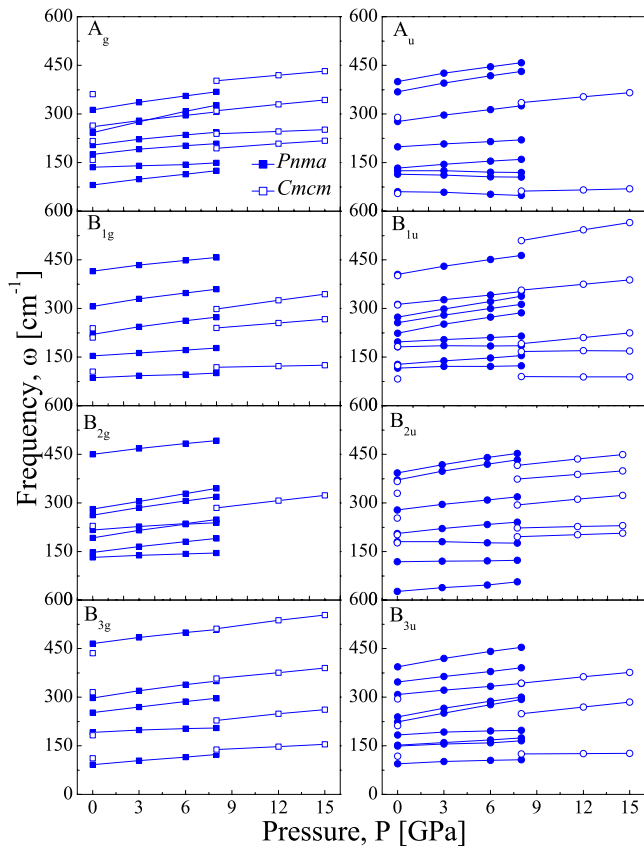


FIG. 3. (Color online) Vibrational behavior as a function of isotropic pressure for  $Pnma$  and  $Cmcm$   $pPv$ . The open and filled symbols are the Raman and the Infra-red modes respectively.

dering (+, +, +, -) could be considered but it is unlikely to appear in real conditions because of the symmetry of the system and the superexchange interaction. For the non-collinearity we have to consider the three Cartesian directions  $x$ ,  $y$  and  $z$  for each magnetic moment which gives  $4 \times 3$  possible states:  $F_x, F_y, F_z, A_x, A_y, A_z, C_x, C_y, C_z, G_x, G_y$  and  $G_z$ . Then, taking into account the fact that the spins are axial vectors, one has to apply the symmetry operations of the  $D_{2h}$  point group on each of the non-collinear magnetic orders defined above and see how they transform. The result of this approach applied on the  $pPv$  phase of  $\text{NaMnF}_3$  is summarised in Table V.

As we can see from Table V, the  $F_x$  and  $A_x$  orders belong to the same character. This means that in an energy expansion with respect to these two order parameters the second order term  $F_x \cdot A_x$  is invariant by symmetry. This implies that if one of the two order parameters condenses in the structure, the second one can develop as well but as a secondary or a slave order (pseudo-proper). This secondary order parameter usually appears as a spin canting in the real system and its intensity will depend on the amplitude of the  $F_x \cdot A_x$  coupling. Going through the other magnetic orders, in Table V we also observe that  $F_y, A_y, C_z$  and  $G_z$  belong to the same  $B_{2g}$  character,  $F_z, A_z,$

TABLE V. Magnetic ordering allowed in the  $Cmcm$  structure according to the  $D_{2h}$  point group.<sup>50,51</sup> The transformation of each magnetic ordering under each symmetry operation is labeled as +1 and -1, which indicates when the ordering is invariant under the related transformation (*i.e.* +1) or when it is reversed under the application of the symmetry operation (*i.e.* -1).

Magnetic Ordering	$I$	$\mathcal{C}_2$	$\mathcal{C}_2$	$\mathcal{C}_2$	$\sigma$	$m_z$	$m_y$	$m_x$
$F_x, A_x$	1	-1	-1	1	1	-1	-1	$B_{3g}$
$F_y, A_y, C_z, G_z$	1	-1	1	-1	1	-1	1	$B_{2g}$
$F_z, A_z, C_y, G_y$	1	1	-1	-1	1	1	-1	$B_{1g}$
$C_x, G_x,$	1	1	1	1	1	1	1	$A_g$

$C_y$  and  $G_y$  belong to the  $B_{1g}$  character and  $C_x$  and  $G_x$  belong to the  $A_g$  character. Interestingly, whatever the main magnetic order we will observe in the  $pPv$  phase of  $\text{NaMnF}_3$ , a canting of the spins is always possible. Additionally, we also remark that three of the four possible characters to which belong all the possible magnetic orders, three of them allow for ferromagnetism and so have the potential to exhibit weak FM.

TABLE VI. Comparison of the distances and the bond angles along the Mn-F-Mn bonds between the  $Pnma$  and the  $Cmcm$  structures of  $\text{NaMnF}_3$ .

Distance and Angle	$Pnma$	$Cmcm$
$d_{Mn-Mn}$ [Å]	[101]	3.9951
	[10-1]	3.9951
	[010]	4.0036
$\gamma_{Mn-F-Mn}$ [deg]	[101]	142.58
	[10-1]	142.58
	[010]	140.14

As discussed above,  $\text{NaMnF}_3$  compound in the  $Pnma$  phase has a  $G$ -type AFM ordering.<sup>41,43,47</sup> In Table VI we report the computed Mn-F-Mn distances and angles of the  $Pnma$  phase at room pressure and of the  $pPv$  phase at 8 GPa. We note that in the  $Pnma$  structure, the Mn-Mn bonding in the three directions have similar Mn-F-Mn angles (about  $140^\circ$ ) and distances (about 4 Å) while they are much more anisotropic in the  $pPv$  phase (angles of  $92^\circ$  and  $134^\circ$  and one non-existent angle due to the octahedral edge sharing of the structure with distances of 2.99 Å and 3.66 Å in the  $x-z$  plane and 4.97 Å in the  $y$  direction). Having angles closer to  $180^\circ$  in the  $Pnma$  explains the  $G$ -type AFM ordering since with such bond angle the superexchange interaction between the Mn- $d^5$  spins favours an AFM alignment.<sup>52-54</sup> In the  $pPv$  case, we can see that there is no direct bonding between the Mn atoms along the  $y$  direction such as we can expect a weak spin coordination between the spins along the  $y$  direction and one would expect a quasi-2D magnetic behaviour in the  $pPv$  structure. In the plane perpendicular to the  $y$  direction we have two types of

bonding giving rise to an angle close to  $180^\circ$  along the  $z$  direction and to an angle close to  $90^\circ$  along the  $x$  direction. On the top of that, we also note that the  $90^\circ$  bonding along the  $x$  direction is given through two bonds since it is the direction where the octahedra share their edge. The superexchange interaction should thus drives strong FM ordering along the  $x$  axis and AFM ordering along the  $z$  axis and a weak interaction along the  $y$  axis. Interestingly, the magnetic ordering that fulfils these superexchange rules is the  $C$ -type AFM and it is indeed the lowest energy collinear magnetic ordering that we found in our calculations (see Fig.4b). Therefore, we can only consider the set of non-collinear calculations containing the  $C$ -type AFM:  $(C_z, F_y, G_z, A_y)$ ,  $(C_y, F_z, A_z, G_y)$  and  $(C_x, G_z)$  as predicted by group theory. We can also expect the  $C_x$  case to be unlikely observed since it forces the spins to be antiferromagnetically aligned along the  $x$  direction while a strong FM interaction is expected from the double  $90^\circ$  bond angle connecting the Mn atoms in this direction.

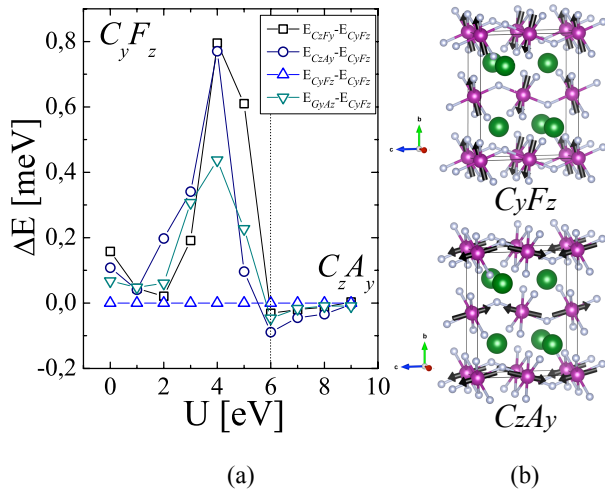


FIG. 4. (Color online) (a) Energy differences between the different magnetic orderings of the  $pPv$  phase of NaMnF<sub>3</sub> versus the  $U$  parameter. (b) Sketch of the  $F_z C_y$  and the  $A_y C_z$  magnetic orderings in the  $pPv$  phase of NaMnF<sub>3</sub>. For  $U < 6.0$  eV the system exhibits a AFM+FM magnetic state with a high ferromagnetic canting. For  $U > 6.0$  eV, the system transit toward a canted AFM state with no weak FM.

Performing the spin relaxations within the non-collinear regime and within the  $C$ -type AFM ordering, we found that the lowest energy is obtained for the  $C_y$  orientation with a large  $F_z$  component along the  $z$  direction (no canting along the  $x$  axis is observed). This magnetic ground state is however dependent on the  $U$  and  $J$  values of the GGA+ $U$  exchange correlation functional. In Fig.4a we report the energy difference between the  $C_y F_z$  ordering and the other lowest energy cases  $C_z F_y$ ,  $C_z A_y$ , and  $G_y A_z$  versus the  $U$  value (fixing  $J = 0$ ). Here we remark that the  $C_y F_z$ ,  $C_z F_y$ ,  $C_z A_y$ , and  $G_y A_z$  states are very close in energy such as we can expect an easy

magnetic phase transitions with small perturbations such as an applied magnetic field. Such a transition under a magnetic field has been observed experimentally in the  $pPv$  phase of NaNiF<sub>3</sub> where a field parallel to the  $y$  axis induces a transition to a AFM+weak-FM ground state.<sup>18</sup> We can see from Fig.4a that the  $C_y F_z$  corresponds to the lowest energy state from  $U = 0.0$  eV to  $U = 5.0$  eV while from  $U = 6.0$  eV to  $U = 9.0$  eV the  $C_z A_y$  is observed to be the most stable. This shows that a magnetic spin flop transition appears in the  $pPv$  phase of NaMnF<sub>3</sub> as function of the electronic Coulomb direct exchange  $U$ . In Fig.5 we report the evolution of the spin canting with respect to  $U$ . The amplitude of the  $F_z$  canting goes from 0.01 to  $1.6 \mu_B$ /atom when varying  $U$  from 0.0 to 9.0 eV. We note that the  $F_z$  component strongly increase from  $U = 0.0$  to 6.0 eV and reach a saturation value beyond  $U = 6.0$  eV. Unfortunately, no experimental data of the non-collinearity of NaMnF<sub>3</sub> in its  $pPv$  phase has been reported in the literature such as it is not possible to validate which  $U$  value would be the best to reproduce the spin canting amplitude. In previous studies with  $d^5$  half filled orbitals the range of  $U$  values that have been found to treat correctly the property of the systems is around  $U = 4.0$  eV. It is important to note that the pressure calculations performed with  $U = 4.0$  eV in the  $Pnma$  and  $pPv$  phase give the best agreement with experiments such as we will use  $U = 4.0$  eV in the rest of our analysis.

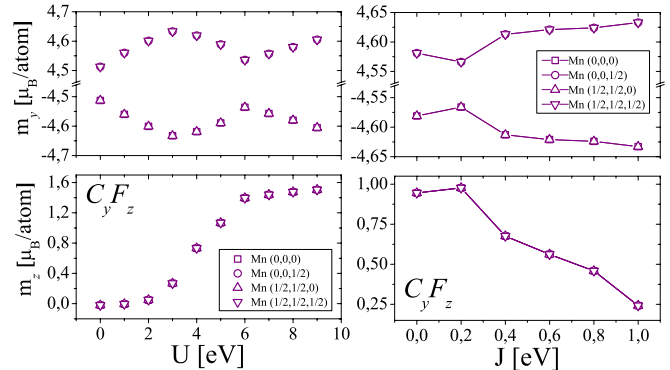


FIG. 5. (Color online) Magnetic canting dependence as a function of  $U$  and  $J$  parameters for NaMnF<sub>3</sub>. Canting angle ( $\varphi$ ) varies from  $0.11^\circ$  to  $17.94^\circ$  when  $U$  goes from 0.0 to 9.0 eV. The canting angle goes from  $12.07^\circ$  to  $3.01^\circ$  when  $J$  varies from 0.0 to 1.0 eV.

Beside the  $U$  parameter, for non-collinear magnetism within the DFT+ $U$  approach it is also necessary to check the dependence with respect to the  $J$  parameter.<sup>55</sup> In Fig.5 we present the evolution of the spin canting versus the  $J$  parameter in the  $C_y F_z$  ground state of the  $pPv$  phase of NaMnF<sub>3</sub> with  $U = 4.0$  eV. As we can see, the FM component  $F_z$  is strongly affected by  $J$ , going from  $0.95 \mu_B$  to  $0.25 \mu_B$  when  $J$  goes from 0.0 to 1.0 eV respectively. Here again, it is difficult to predict what would be the best  $J$  value for NaMnF<sub>3</sub> without any experimental feedback. Previous studies about the DFT+ $U$   $J$  parameter report that low  $J$  values for  $d^5$  orbital filling are

usually the best values<sup>55</sup> such as the large values of the  $F_z$  canting we obtain at low  $J$  (close to  $1 \mu_B/\text{atom}$ ) in the  $pPv$  phase of  $\text{NaMnF}_3$  would be the optimized value.

In order to estimate the error bar of our calculations, we report in Table VII a list of known magnetic  $pPv$  phase in oxide and fluoride perovskites with their related magnetic orderings,  $d$  orbital filling and  $S$  quantum number. We note that in all oxide cases as well as in  $\text{NaNiF}_3$ , the ground state spin configuration always corresponds to the low spin state. According to our calculations, only  $\text{NaMnF}_3$  has the high spin configuration as ground state. In order to verify if this is due to the DFT parameters used in our calculations or if this has a physical meaning, we performed calculations of the  $pPv$  phase of  $\text{NaNiF}_3$  and  $\text{CaRhO}_3$  with  $U=4.0$  eV. We found a low spin ground state in both  $\text{NaNiF}_3$  ( $S=1$ ) and  $\text{CaRhO}_3$  ( $S=\frac{1}{2}$ ) and so in good agreement with the experimental results. Going further, we also estimated the non-collinear spin ground state of  $\text{NaNiF}_3$  and  $\text{CaRhO}_3$  in their  $pPv$  phase. As expected from the symmetry analysis, we observe canted magnetic ground state in the two systems. The ground state magnetic ordering of  $\text{NaNiF}_3$  is found to be  $A_z$  with a  $G_y$  canting. Then, we did not find any weak ferromagnetic spin canting in  $\text{NaNiF}_3$  in agreement with the experimental data. We note that experimentally a transition toward an AFM state with a ferromagnetic canting is observed in the  $pPv$  phase of  $\text{NaNiF}_3$  when applying a small magnetic field. The direction of the field induced canted FM spins in  $\text{NaNiF}_3$  are the same than the one we report in the  $pPv$  phase of  $\text{NaMnF}_3$  without magnetic field. This shows that the high-spin large FM canting we report in  $\text{NaMnF}_3$  might be metastable in  $\text{NaNiF}_3$  such as a small magnetic perturbation can switch to this state. More theoretical and experimental analysis would be welcome to understand this transition. In the case of  $\text{CaRhO}_3$  we found  $C_y$  with a  $F_z$  canting as magnetic ground state.

No experimental measurements of the amplitude of the spin canting has been reported for  $pPv$   $\text{CaRhO}_3$  and  $\text{NaNiF}_3$  but we found that when considering the cases with ferromagnetic spin canting, the canting angle is much smaller in  $\text{CaRhO}_3$  ( $4.3^\circ$ ) and in  $\text{NaNiF}_3$  ( $4.7^\circ$ ) than it is in  $\text{NaMnF}_3$  ( $11.7^\circ$ , see Table VIII). If we look at the amplitude of the canting per atom we observe a very large amplitude for  $\text{NaMnF}_3$  ( $0.95 \mu_B/\text{atom}$ ) due to the high spin configuration while it is much smaller in the case of  $\text{NaNiF}_3$  ( $0.12 \mu_B/\text{atom}$ ) and of  $\text{CaRhO}_3$  ( $0.05 \mu_B/\text{atom}$ ). This large canting can be the result of a rather large Dzyaloshinsky-Moriya interaction<sup>56,57</sup> or a large single-ion anisotropy<sup>58</sup> and more detailed analysis would be required in order to identify the exact origin of this large spin canting. These calculations allow us to be more confident about the unique high spin ground state of  $\text{NaMnF}_3$  with a large ferromagnetic spin canting in its  $pPv$  phase.

We also report in Fig.6 the local density of states (LDOS) of the  $pPv$  phase of  $\text{NaMnF}_3$ . The LDOS shows an overlap between the Mn- $3d$  and F- $2p$  states, suggest-

TABLE VII. Magnetic ordering in fluorides and oxides post-perovskite systems, AFM: antiferromagnetic, DM: diamagnetic, FM: ferromagnetic, CWP: Curie-Weiss paramagnetic. \* $\text{NaNiF}_3$  compound present a magnetic transition from AFM to AFM+FM ordering at applied external magnetic field<sup>18</sup>. \*\*This work. All  $pPv$  compounds exhibit a low-spin magnetic configuration but  $\text{NaMnF}_3$  that according to our calculations is found to be in the high-spin state.

Compound	Magnetic ordering			ref
<i>pPv</i> Oxides $ABO_3$				
$\text{CaIrO}_3$	quasi-1D AFM	$S=\frac{1}{2}$	$\text{Ir}^{4+}: 5d^5(\text{LS})$	20
$\text{CaRuO}_3$	quasi-1D AFM	$S=1$	$\text{Ru}^{4+}: 4d^4(\text{LS})$	22,24
$\text{CaPtO}_3$	DM	$S=0$	$\text{Pt}^{4+}: 5d^6(\text{LS})$	25,26
$\text{CaRhO}_3$	AFM+weak-FM	$S=\frac{1}{2}$	$\text{Rh}^{4+}: 4d^5(\text{LS})$	28
$\text{NaIrO}_3$	CWP	$S=1$	$\text{Ir}^{5+}: 5d^4(\text{LS})$	29
<i>pPv</i> Fluorides $ABF_3$				
$\text{NaCoF}_3$	AFM	—	$\text{Co}^{2+}: 3d^7(\text{LS})$	16
$\text{NaNiF}_3$	AFM*	$S=1$	$\text{Ni}^{2+}: 3d^8(\text{LS})$	18,**
$\text{NaMnF}_3$	AFM+FM	$S=\frac{5}{2}$	$\text{Mn}^{2+}: 3d^5(\text{HS})$	**

TABLE VIII. Magnetic orderings allowed in the  $Cmcm$  structure for  $ABX_3$  systems with  $U = 4.0$  eV and  $J = 0$ . The large magnetic canting for fluorides compounds can be noted. The canting angle ( $\varphi$ ) is measured with respect to the  $ab$ -plane on the  $pPv$  phase. For  $\text{NaNiF}_3$ , the two possible magnetic states  $C_z F_y$  and  $C_y F_z$  were computed.

Compound	$F_i$ [ $\mu_B/\text{atom}$ ]	$\varphi$ [deg]	Magnetic Ground-state
$\text{CaRhO}_3$	0.05	4.3	$C_y F_z$
$\text{NaNiF}_3$	0.12 (0.15)	86.1 (4.7)	$C_z F_y$ ( $C_y F_z$ )
$\text{NaMnF}_3$	0.95	11.7	$C_y F_z$

ing a covalent contribution between the Mn and F atoms due to the  $p-d$  hybridization, which is a fundamental requirement for the superexchange interaction. Moreover, we observe that the fluorine states are lower in energy than the Mn- $d$  orbitals, which corresponds to the expected bonding-antibonding picture of covalency between magnetic cations and anions. Close to the Fermi level, no contribution of Na states to the DOS is observed such as mostly Na size effects are expected within the structure, a key-point parameter that is at the origin of the geometric ferroelectric instabilities observed in cubic fluoroperovskites.<sup>19</sup> The  $d_{xy}$ ,  $d_{xz}$ ,  $d_{yz}$ ,  $d_{z^2}$  and  $d_{x^2-y^2}$  orbital occupancy gives the 5 orbitals filled below the Fermi level for a spin channel and the 5 orbitals empty above of the Fermi level for the other spin channel, which confirms the high spin electronic configuration of  $\text{Mn}^{2+}$  in the  $pPv$  phase of  $\text{NaMnF}_3$ .

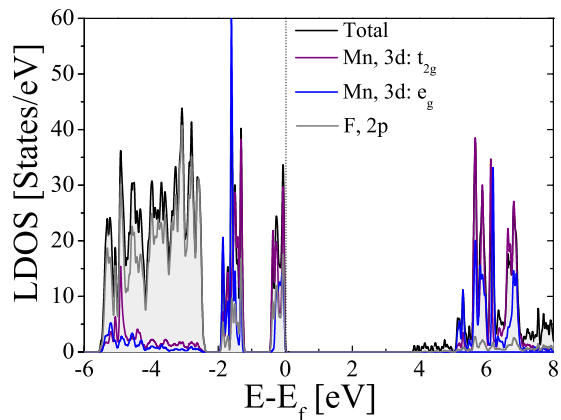


FIG. 6. (Color online) Projected local density of states (LDOS) of the  $Cmcm$  phase of  $\text{NaMnF}_3$ . A regular F- $p$  bonding Mn- $d$  antibonding is observed with small Mn:3d – F:2p overlapping DOS is responsible for the small superexchange interaction present in  $\text{NaMnF}_3$ .

### Conclusions

We have studied by means of first-principles calculations the high pressure phase diagram of  $\text{NaMnF}_3$ . We predicted a phase transition from the  $Pnma$  distorted perovskite to a  $Cmcm$  post-perovskite phase at a critical pressure of 8 GPa which is relatively low with respect to the similar phase transition observed in other compounds. As proposed by O’Keeffe<sup>45</sup> this phase transition fits very well with the octahedra tilting angle requirements where the transition to the  $pPv$  is observed when the octahedra tilting angle reach the critical value of  $25^\circ$  with an initial ambient pressure tilting angle of  $15^\circ$ . Unfortunately high pressure experiments have been performed at very high temperature by Akaogi *et. al.*<sup>44</sup> where the O’Keeffe requirement is not fulfilled and also by Katrusiak *et. al.*<sup>47</sup> who unfortunately did not go beyond 5 GPa such as none of them observed the  $pPv$  transition. Because of the partially filled  $d$  orbitals of  $\text{Mn}^{2+}$  cation we also determined the magnetic ground state of  $\text{NaMnF}_3$  in its  $pPv$  phase. Our calculations predicted a

high spin ground state of the  $d^5$  spins with a magnetic moment of  $5\mu_B$  on each Mn. This high spin structure is particularly interesting and unique since all the other known magnetic compounds presenting the  $pPv$  phase present a low spin ground state. We predicted an AFM magnetic ordering ground state of the  $C$  type with the spins lying along the  $y$  direction and with a surprisingly large ferromagnetic spin canting along the  $z$  direction. This makes  $\text{NaMnF}_3$  of particular interest for fundamental and geophysical studies since it has this unique property of high spin magnetic ground state with potentially large ferromagnetic spin canting and because it can be synthesized at relatively small pressure. The fact that the fluoride postperovskites can be maintained when the pressure is released makes  $\text{NaMnF}_3$  even more interesting to study. We hope that our results will motivate the experimentalist to carry out more studies of  $\text{NaMnF}_3$  in order to confirm the  $pPv$  phase transition at low pressure and low temperature and to check its potential for high spin structure with a sizeable canted ferromagnetism.

### Acknowledgements

This work used the Extreme Science and Engineering Discovery Environment (XSEDE), which is supported by National Science Foundation grant number OCI-1053575 as well as the machines of the Consortium des Equipements de Calcul Intensif (CECI) Funded by F.R.S.-FNRS Belgium. Additionally, the authors acknowledge the support from the and Texas Advances Computer Center (TACC) and Super Computing System (Mountaineer) at WVU, which are funded in part by the National Science Foundation EPSCoR Research Infrastructure Improvement Cooperative Agreement 1003907, the state of West Virginia (WV EPSCoR via the Higher Education Policy Commission) and WVU. A.H. Romero and A.C. Garcia-Castro acknowledge the support of the Marie Curie Actions from the European Union in the international incoming fellowships (grant PIIFR-GA-2011-911070) and CONACyT project 152153. This work was also supported by F.R.S.-FNRS Belgium (EB).

<sup>1</sup> R. Cohen, *Nature* **358**, 136 (1992).

<sup>2</sup> D. Khomskii, in *Spin Electronics*, Lecture Notes in Physics, Vol. 569, edited by M. Ziese and M. Thornton (Springer Berlin Heidelberg, 2001) pp. 89–116.

<sup>3</sup> G. Sági-Szabó, R. E. Cohen, and H. Krakauer, *Phys. Rev. Lett.* **80**, 4321 (1998).

<sup>4</sup> A. N. Morozovska, E. A. Eliseev, M. D. Glinchuk, L.-Q. Chen, and V. Gopalan, *Phys. Rev. B* **85**, 094107 (2012).

<sup>5</sup> C. N. R. Rao, *Ferroelectrics* **102**, 297 (1990).

<sup>6</sup> I. Žutić, J. Fabian, and S. Sarma, *Rev. Mod. Phys.* **76**, 234 (2004).

<sup>7</sup> H. Bea, M. Gajek, M. Bibes, and A. Barthemy, *J. Phys. Cond. Matter* **20**, 434221 (2008).

<sup>8</sup> P. Zubko, S. Gariglio, M. Gabay, P. Ghosez, and J.-M. Triscone, *Annual Review of Condensed Matter Physics* **2**, 141 (2011).

<sup>9</sup> Y.-H. Chu, L. W. Martin, M. B. Holcomb, and R. Ramesh, *Materials Today* **10**, 16 (2007).

<sup>10</sup> R. J. Angel, J. Zhao, and N. L. Ross, *Phys. Rev. Lett.* **95**, 025503 (2005).

<sup>11</sup> M. Murakami, K. Hirose, K. Kawamura, N. Sata, and Y. Ohishi, *Science (New York, N.Y.)* **304**, 855 (2004).

<sup>12</sup> T. Tsuchiya, J. Tsuchiya, K. Umemoto, and R. M. Wentzcovitch, *Earth and Planetary Science Letters* **224**, 241 (2004).

<sup>13</sup> K. Hirose, *American Mineralogist* **90**, 262 (2005).

- <sup>14</sup> S. Tateno, K. Hirose, N. Sata, and Y. Ohishi, *Phys. Chem. Minerals* **32**, 721 (2005).
- <sup>15</sup> C. D. Martin, W. a. Crichton, H. Liu, V. Prakapenka, J. Chen, and J. B. Parise, *American Mineralogist* **91**, 1703 (2006).
- <sup>16</sup> H. Yusa, Y. Shirako, and M. Akaogi, *Inorg. Chem.* **51**, 6559 (2012).
- <sup>17</sup> D. P. Dobson, S. a. Hunt, A. Lindsay-Scott, and I. G. Wood, *Physics of the Earth and Planetary Interiors* **189**, 171 (2011).
- <sup>18</sup> Y. Shirako, Y. Shi, A. Aimi, and D. Mori, *J. Solid State ...* **191**, 167 (2012).
- <sup>19</sup> A. C. Garcia-Castro, N. A. Spaldin, A. H. Romero, and E. Bousquet, *Phys. Rev. B* **89**, 104107 (2014).
- <sup>20</sup> N. A. Bogdanov, V. M. Katukuri, H. Stoll, J. van den Brink, and L. Hozoi, *Phys. Rev. B* **85**, 235147 (2012).
- <sup>21</sup> T. B. Ballaran, R. G. Tronnes, and D. J. Frost, *American Mineralogist* **92**, 1760 (2007).
- <sup>22</sup> Y. Shirako, H. Satsukawa, H. Kojitani, T. Katsumata, M. Yoshida, Y. Inaguma, K. Hiraki, T. Takahashi, K. Yamaura, E. Takayama-Muromachi, and M. Akaogi, *J. Phys.: Conference Series* **215**, 012038 (2010).
- <sup>23</sup> H. Kojitani, Y. Shirako, and M. Akaogi, *Phys. Earth and Planetary Interiors* **165**, 127 (2007).
- <sup>24</sup> Y. Shirako, H. Satsukawa, X. X. Wang, J. J. Li, Y. F. Guo, M. Arai, K. Yamaura, M. Yoshida, H. Kojitani, T. Katsumata, Y. Inaguma, K. Hiraki, T. Takahashi, and M. Akaogi, *Phys. Rev. B* **174411**, 1 (2011).
- <sup>25</sup> K. Ohgushi, Y. Matsushita, N. Miyajima, Y. Katsuya, M. Tanaka, F. Izumi, H. Gotou, Y. Ueda, and T. Yagi, *Phys. Chem. Minerals* **35**, 189 (2008).
- <sup>26</sup> Y. Inaguma, K.-i. Hasumi, M. Yoshida, T. Ohba, and T. Katsumata, *Inorg. Chem.* **47**, 1868 (2008).
- <sup>27</sup> Y. Shirako, H. Kojitani, M. Akaogi, K. Yamaura, and E. Takayama-Muromachi, *Phys. Chem. Minerals* **36**, 455 (2009).
- <sup>28</sup> K. Yamaura, Y. Shirako, H. Kojitani, M. Arai, D. P. Young, M. Akaogi, M. Nakashima, T. Katsumata, Y. Inaguma, and E. Takayama-Muromachi, *J. Am. Chem. Soc.* **131**, 2722 (2009).
- <sup>29</sup> M. Bremholm, S. E. Dutton, P. W. Stephens, and R. J. Cava, *J. Solid State Chem.* **184**, 601 (2011).
- <sup>30</sup> S. Yakovlev, M. Avdeev, and M. Mezouar, *J. Solid State Chem.* **182**, 1545 (2009).
- <sup>31</sup> G. Kresse and J. Furthmüller, *Phys. Rev. B* **54**, 11169 (1996).
- <sup>32</sup> G. Kresse, *Phys. Rev. B* **59**, 11 (1999).
- <sup>33</sup> P. Blochl, *Phys. Rev. B* **50**, 953 (1994).
- <sup>34</sup> J. Perdew, A. Ruzsinszky, G. Csonka, O. Vydrov, G. Scuseria, L. Constantin, X. Zhou, and K. Burke, *Phys. Rev. Lett.* **100**, 1 (2008).
- <sup>35</sup> A. Liechtenstein, V. Anisimov, and J. Zaanen, *Phys. Rev. B* **52**, 5467 (1995).
- <sup>36</sup> D. Hobbs and G. Kresse, *Phys. Rev. B* **62**, 556 (2000).
- <sup>37</sup> F. Birch, *Phys. Rev.* **71**, 809 (1947).
- <sup>38</sup> X. Gonze, *Phys. Rev. A* **52**, 1086 (1995).
- <sup>39</sup> X. Gonze, *Phys. Rev. A* **52**, 1096 (1995).
- <sup>40</sup> A. Togo, F. Oba, and I. Tanaka, *Phys. Rev. B* **78**, 1 (2008).
- <sup>41</sup> P. Daniel, M. Rousseau, A. Desert, A. Ratuszna, and F. Ganot, *Phys. Rev. B* **51**, 12337 (1995).
- <sup>42</sup> A. Lane, D. Sharp, and J. Barraclough, *J. Chem. Soc.* **94**, 94 (1971).
- <sup>43</sup> J. R. Shane, *J. Appl. Phys.* **38**, 1280 (1967).
- <sup>44</sup> M. Akaogi, Y. Shirako, H. Kojitani, T. Nagakari, H. Yusa, and K. Yamaura, *Phys. Earth and Planetary Interiors* , (2013).
- <sup>45</sup> M. O'keeffe, B. Hyde, and J. Bovin, *Phys. Chem. Minerals* **305**, 299 (1979).
- <sup>46</sup> S. Tateno, K. Hirose, N. Sata, and Y. Ohishi, *Phys. Earth and Planetary Interiors* **181**, 54 (2010).
- <sup>47</sup> A. Katrusiak and A. Ratuszna, *Solid State Comm.* **84**, 435 (1992).
- <sup>48</sup> B. Beznosikov and K. Aleksandrov, *Crystallography Reports* **45**, 792 (2000).
- <sup>49</sup> D. Babel and A. Tressaud, in *Inorganic Solid Fluorides*, edited by P. Hagenmuller (Academic Press, 1985) pp. 77 – 203.
- <sup>50</sup> M. Aroyo, L. J. M. Perez-Mato, C. Capillas, E. Kroumova, S. Ivantchev, G. Madariaga, A. Kirov, and H. Wondratschek, *Zeitschrift für Kristallographie - Crystalline Materials* **221**, 15 (2009).
- <sup>51</sup> M. I. Aroyo, A. Kirov, C. Capillas, J. M. Perez-Mato, and H. Wondratschek, *Acta Cryst* **62**, 115 (2006).
- <sup>52</sup> J. Kanamori, *Prog. Theor. Phys.* **17**, 177 (1957).
- <sup>53</sup> J. Kanamori, *Prog. Theor. Phys.* **17**, 197 (1957).
- <sup>54</sup> J. B. Goodenough, *J. Phys. and Chem. Solid.* **6**, 287 (1958).
- <sup>55</sup> E. Bousquet and N. Spaldin, *Phys. Rev. B* **82**, 220402 (2010).
- <sup>56</sup> I. Dzyaloshinsky, *J. Phys. and Chem. Solid.* **4**, 241 (1958).
- <sup>57</sup> T. Moriya, *Phys. Rev.* **120**, 91 (1960).
- <sup>58</sup> G. Maekawa, S., Tohyama, T., Barnes, S.E., Ishihara, S., Koshibae, W., Khaliullin, *Physics of Transition Metal Oxides* (Springer, Berlin, 2004).